REVISTA MATÉRIA
V.24 N.03
ISSN 1517-7076 artigos e-12459, 2019

Effect of Sigma Phase Precipitated at 850 °C on Corrosion Behaviour of UNS S82441 Duplex Stainless Steel

Daniel Amâncio Cavalcanti [1], Palloma Vieira Muterlle [1], Gustavo Reinke [1]

[1] Department of Mechanical Engineering, Faculty of Technology, University of Brasília, UnB, 70910-900, Brasília, Distrito Federal, Brasil.
e-mail: danielcavalcanti84@gmail.com, pmuterlle@gmail.com, gustav.reinke@gmail.com

ABSTRACT

Duplex stainless steels (DSS) are alloys with binary microstructure consisting of ferrite (δ) and austenite (γ), combining high mechanical properties and corrosion resistance by pitting and stress corrosion, due to the two phases austenite/ferrite. However, the formation of secondary and intermetallic phases, during solidification processes, heat treatment or welding in duplex steels tend to cause the degradation of its main properties. The present study aim to investigate the corrosion behaviour of UNS S82441 aged at 850°C for 30, 300 and 3000 minutes, due to the formation of sigma phase. Corrosion resistance evaluation was performed by means of stress corrosion testing, potenciodinamic polarization and mass loss. The microstructural characterization and morphology confirmed the presence of sigma phase in the UNS S82441 duplex stainless steel, and that the amount of this phase increases with the time of heat treatment of aging. The aging time influences negatively the corrosion resistance of this steel, with a gradual drop of up to 50% on passivation regime for the condition of aging at 850°C for 3000 minutes.

Keywords: Duplex Stainless Steel. Corrosion. Sigma Phase. Heat Treatment of Aging.

1. INTRODUCTION

Duplex stainless steels (DSS) are system alloys Fe-Cr-Ni-Mo, 50% ferrite (δ) and 50% austenite (γ), with similar amounts of δ/δ and γ/γ grain boundaries, and δ/γ interfaces [1-3]. Especially in industries of oil prospecting, oil refining, petrochemical and energy, there is a great attraction for the use of duplex steels due to the combination of corrosion resistance and high mechanical properties, mainly in aggressive environments for steels [2,3]. However, these properties can be drastically reduced, if undesirable secondary phases formations occur, such as sigma phase (σ), chi phase (χ), austenite (γ2), chromium nitrides (Cr2N) and carbides (M23C6, M7C3). The high corrosion resistance of DSS derives from their high Cr content in combination with additions of Mo, Ni and N [4]. However, high molybdenum levels increase the tendency for deleterious precipitates to form. The intermetallic phases cited remove elements such as chromium (Cr) from the alloy matrix [4,5]. The sigma phase is a tetragonal crystal structure that has particular impact on the reduction of corrosion resistance and mechanical properties of DSS, having deleterious effect such as embrittlement [4-8]. The precipitation of σ phase in stainless steels occurs between 600°C and 1000°C, its precipitation being faster between 800°C and 900°C due to the eutectoid decomposition of ferrite to sigma ($\delta \rightarrow \sigma$), in the high Cr-concentrated region of δ (above 20 wt.%) [7-9]. The sigma phase takes place at high-energy regions such as grain boundaries and interfaces (δ/δ and δ/γ). After nucleation, sigma grows into ferrite phase, it is because an interstitial atom (Cr) can diffuse faster in a body-centred cubic structure (δ-BCC) than in face-centred cubic structure (γ-FCC) [6-8].

Recent developments in stainless steels led to the evolution of the subgroup of duplex stainless steels known as Lean Duplex Stainless Steels (LDX or LDSS). It has less content of alloying elements in relation to standard DSS, and therefore, lower cost plus greater corrosion resistance combined with mechanical properties about twice higher than the austenitic stainless steels [3,10]. A better combination of mechanical properties and corrosion resistance of DSS occurs when austenite is maintained between 40-60% [1-3]. In contrast to traditional DSS, the Outokumpu company developed the Lean Duplex Stainless Steel LDX-2404® in 2010, which became available as UNS S82441 by the ASTM in 2011 [11]. Compared to the study of DSS, studies about LDSS are still incipient, focusing primarily on 2304 and 2204, most common commercially. Due to

Autor Responsável: Daniel Amâncio Cavalcanti Data de envio: 13/04/2018 Data de aceite: 09/01/2019

10.1590/S1517-707620190003.0775

recently DSS developments, it is necessary to investigate the corrosion behaviour of UNS S82441 LDSS, recently developed, as well as the effects of precipitates in its properties.

The present study aims to investigate the effect of sigma phase in corrosion resistance of UNS S82441 LDSS after heat treatment of the aging at 850°C for different times (30, 300 and 3000 minutes).

2. EXPERIMENTAL METHOD

The material was supplied as cold rolled 3 mm thickness plate. Samples were produced for microstructural characterization and corrosion tests. The chemical composition of the material was determined by Energy Dispersive Spectrometry, in semi quantitative analysis, coupled with the Scanning Electron Microscope (SEM-EDS, Model JEOL JSM-7100F). Analysed 10 distinct regions, the results are presented in Table 1.

Table 1: Chemical composition (wt%) of UNS S82441 LDSS (SEM-EDS).

ELEMENT	WT%
Fe	61,73 ± 1,40
Cr	24,52 ± 1,08
Ni	3,69 ± 0,66
Mo	1,91 ± 0,54
Mn	2,51 ± 0,87
N	0,12 ± 0,17
Cu	0,31 ± 0,12

2.1 Aging Thermal Treatments

Isothermal treatments were carried out in an electric furnace muffle at 850°C, with a temperature variation of ± 2 °C, for 30, 300 and 3000 minutes. After the isotherm times, all samples were quickly cooled in water.

2.2 Microstructural Characterization

Specimens of 10 x 10 x 3 mm were cut from the plate for microscopy. All samples were ground, using grinding papers between 400 and 2500 mesh, followed by polishing with diamond paste 3 μm and 1 μm. The microstructure was investigated by confocal laser microscope (CONFOCAL, Model Olympus LEXT, OLS-4100) after etching with Modified Behara reagent (80 ml H2O, 20 ml HCl, 1g K2S2O5, 2g NH4HF2) for 15 to 60 s. For quantification of the phases, the methodology described in the ASTM E1245-03 standard was used as reference, using the ImageJ v.1.51® software. The crystal structures were analysed by using X-ray diffraction (XRD, Model Shimadzu LabX XRD-6000 diffractometer) with Cu-Kα radiation, 40 kV voltage and 30 mA current. XRD data were collected in a range of Bragg's angles ($10° \leq 2\theta \leq 100°$), with 2°/min speed.

2.3 Corrosion Tests

To investigate the influence of the sigma-phase precipitation on the corrosion behaviour, the following experimental techniques were used: (a) open circuit potential (OCP); (b) potentiodynamic polarization; (c) stress corrosion cracking (SCC); and (d) mass loss. The Table 2 shows the test solutions used.

Table 2: Solution and temperatures used in corrosion tests.

TEST	SOLUTION (Wt%)	TEMPERATURE (°C)
OCP	NaCl (3,0%)	25 ± 2
Potentiodynamic Polarization	NaCl (3,0%)	25 ± 2
SCC	$MgCl_2$ (43%)	155 ± 2
Mass Loss	$FeCl_3$ (6%)	50 ± 2
Pickling	HNO_3 (20%) + HF (5%)	60 ± 2

The electrochemical tests were performed using a potentiostat/galvanostat (Model METROHM AUTOLAB) and a conventional electrochemical cell with three electrodes immersed the 3% NaCl solution. A saturated calomel electrode was used as the reference electrode. A platinum counter electrode was also used. UNS S82441 samples (exposed area of 1 cm²) mounted in thermoset resin were used as working electrode, and the potential was swept in the anodic direction (according to ASTM G5).

1. Open circuit potential (OCP): The open circuit potential (corrosion potential) of the specimens was monitored for 1200s in the 3% sodium chloride solution, in triplicate for each sample.
2. Potentiodynamic polarization: The tests were carried out using a scan rate of 0.1 mV/s and a range of potential investigated was - 100mV to + 1,6V, in relation to the corrosion potential (E_{cor}) determined by the OCP measured.
3. Stress corrosion cracking: U-bend specimens were shaped according to ASTM G30. Specimens with dimension 100 x 10 x 3 mm were cut and bended. The specimens were stressed using a two-stage method around a cylindrical rod with a 26 mm diameter, and secured with nuts and bolts. Two U-Bend specimens immersed in effervescent magnesium chloride solution were used at 155°C for 24 hours, as prescribed in ASTM G36, for each studied condition.
4. Mass loss: Specimens with dimension 50 x 20 x 3 mm were immersed in a ferric chloride solution at 50°C ± 2 °C for 24 hours. Before and after immersion, the samples were pickled (in solution 20% HNO_3 + 5% HF, 60°C) for 5 minutes. The samples mass were measured before and after immersion.

3. EXPERIMENTAL RESULTS

3.1 Microstructural Characterization

Figure 1a shows typical microstructures found in the solution treated DSS specimens, containing only austenite and ferrite; the ferrite content of the solution treated sample is 51.91 ± 5.52%. Austenite "islands" elongated in the rolling direction were dispersed in the δ-ferrite matrix; the austenite content of the solution treated sample is 48.10 ± 5.25%. The presence of precipitates is not evident.

Aged samples showed sigma phase formation always associated with ferrite-austenite interfaces (Figure 1b). Figure 1c shows that the intermetallic phase started to grow towards ferrite, evidencing the consumption of ferrite for the formation of the sigma precipitate ($\delta \rightarrow \sigma$). Long-term aging increased in the number of sites of austenite; the austenite content of the 3000 minutes aged at 850°C sample is 56,50% ± 6,92%, possibly due to the formation of secondary austenite in the micro regions that was total ferrite consumption ($\delta \rightarrow \sigma + \gamma 2$). Figure 1d shows the increase in the fraction of the sigma phase until reaching a volume fraction almost equal to that of the ferrite in the microstructure, for the condition of aging for the longer time (3000 minutes).

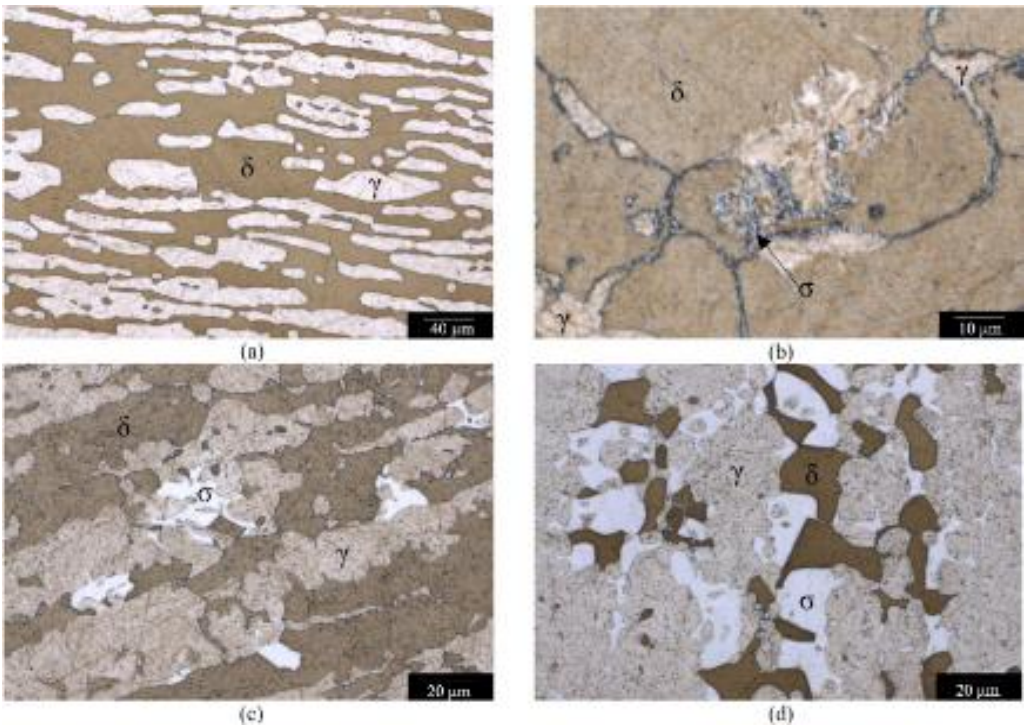

Figure 1: Microstructure of UNS S82441 LDSS studied after modified Behara etching (1000X): (a) as-received (rolling direction); aged at 850°C for: (b) 30 minutes; (c) 300 minutes; (d) 3000 minutes (through thickness direction).

A quantitative stereological analysis was performed to determine the area fraction occupied by each phase. The stereological analysis was based on ASTM E1245-03. Ten fields of each sample were analysed and *ImageJ*® software was used for quantification. Table 3 shows the mean volume fractions occupied by each phase, for each treatment time, obtained from the laser confocal microscopy images. As expected, there was an increase in the intermetallic phase volumetric fraction, for longer treatment times.

Table 3: Volumetric fractions of the phases (%).

AGING TIME (MIN)	AUSTENITE (Γ)	FERRITE (Δ)	SIGMA (Σ)
0	48,10% ± 5,25%	51,91% ± 5,52%	0
30	44,61% ± 3,71%	53,50% ± 3,87%	1,89% ± 0,81
300	46,31% ± 4,68%	49,18% ± 4,73%	4,51% ± 1,41
3000	56,50% ± 6,92%	23,36% ± 5,58%	20,14% ± 2,52

Scanning electron microscopy analysis was used to distinguish between the phases in the samples using the backscattered electron signal. Three different phases were identified from the EDS spectra, as shown on Figure 2. Comparison with results reported in the literature confirmed that the precipitate corresponded to the sigma phase, due to the highest levels of Cr. The distinction between austenite and ferrite was based on the difference in the Ni and Cr contents of these phases [12]. On Table 4 it is shown the results of the chemical composition analysis for points of each phase.

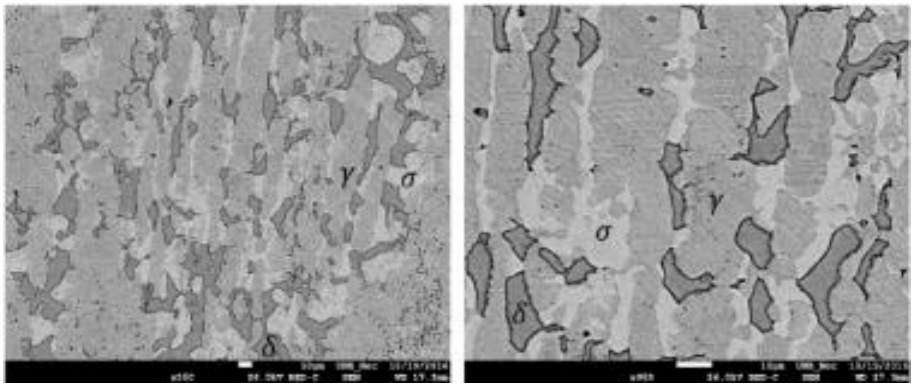

Figure 2: SEM of UNS S82441 LDSS aged 3000 minutes at 850 °C.

Table 4: Chemical compositions of the γ, δ, and σ phases quantified by SEM-EDS.

5. PHASE	CHEMICAL COMPOSITIONS (WT%)					
	Cr	Ni	Mo	Mn	N	Cu
Ferrite	24,75 ± 0,41	2,38 ± 0,38	2,48 ± 0,21	1,80 ± 0,04	0	0,45 ± 0,08
Austenite	21,48 ± 0,69	4,30 ± 0,18	1,41 ± 0,08	2,66 ± 0,18	0,82 ± 0,07	0,55 ± 0,06
Sigma	31,36 ± 0,01	2,16 ± 0,19	4,88 ± 0,06	2,04 ± 0,11	0	0,21 ± 0,07

To confirm the presence of the phases observed by microscopy, X-ray diffraction analysis was performed. As results, the diffraction spectra shown in Figure 3 were obtained.

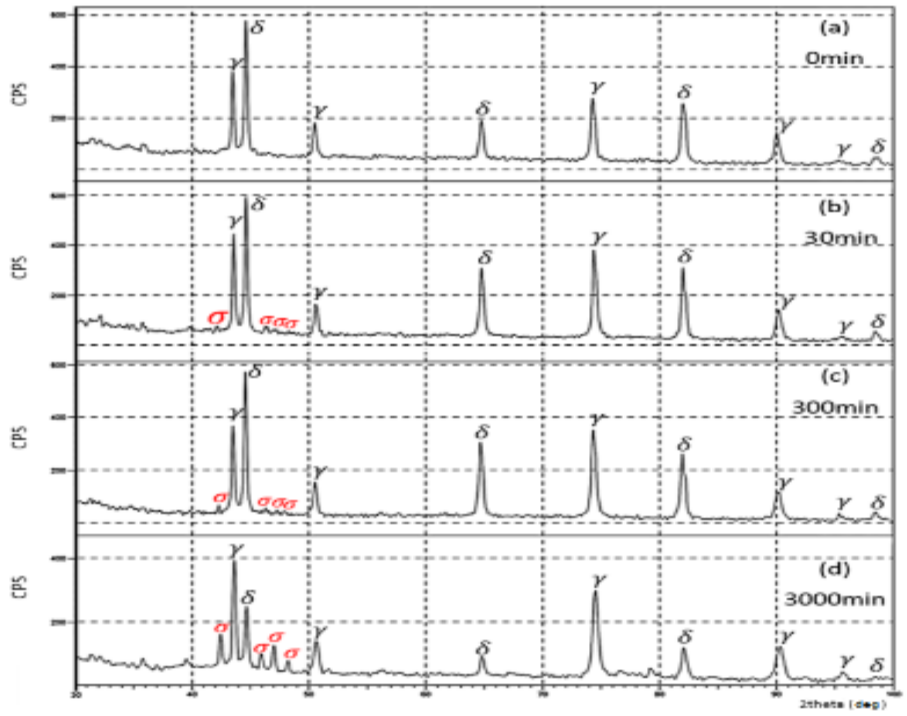

Figure 3: UNS S82441 LDDD diffractograms: (a) as-received; aged at 850°C for (b) 30 min; (c) 300 min; (d) 3000min

The diffractogram of Figure 3a (as-received material), presents the ferrite and austenite phases with peaks corresponding to 2θ and respective Miller indices: 44.69° (110), 64.71° (200) and 81.98° (211) for the ferrite phase; and 43.46° (111), 50.47° (200), 74.25° (220) and 89.99° (311) for the austenite phase, no peaks of intermetallic phases are observed, indicating that the material was supplied in solubilized state. The aged

specimens present a repetition of the peaks corresponding to the austenite and ferrite phases; however present sigma phase peaks, corresponding to 42.42° (410); 44.89° (420); 46.99° (411) and 48.19° (331). The diffractogram of Figure 3d shows the highest intensities for the sigma phase peaks at 850°C for 3000 minutes, compared to the samples aged for 30 and 300 min, accompanied by a reduction in the intensity of the peaks of ferrite phase.

3.2 Electrochemical Corrosion Testing

The evolution of open circuit potentials (OCP) for each heat treatment condition monitored versus time in 3.0% NaCl solution (room temperatura) is shown in Figure 4. The open circuit potentials of samples moved towards the more positive potentials over time and tended to stabilize, exhibiting typical behavior of passive material.

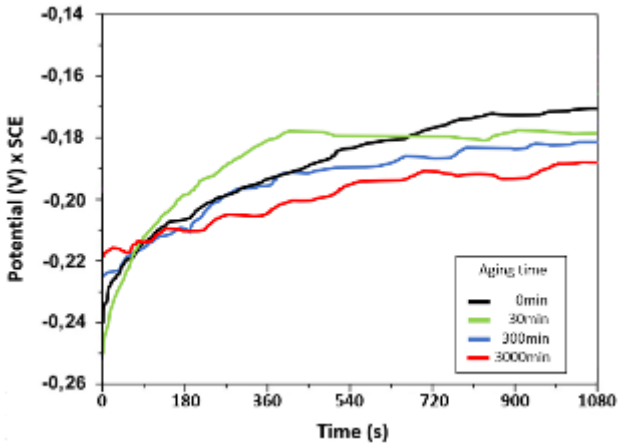

Figure 4: OCP (V) versus time (seconds) for all samples at room temperature in 3% NaCl.

Due to the concentration of Cr and Mo in the sigma phase, which are important elements in the formation of the passive layer, the lowest values of open circuit potential (according to Table 5), absolute and on average, were observed for the highest level of sigma precipitate (σ) which indicates higher surface activity in this condition. Surface heterogeneity and the presence of ions acting in the areas of failure in passivation due to precipitation can cause areas of potential difference leading to galvanic cells.

The potentiodynamic polarization curves of UNS S82441 LDSS measured in 25°C, 3,0% NaCl solution at the scan rate of 0,01mV/s are shown in Figure 5.

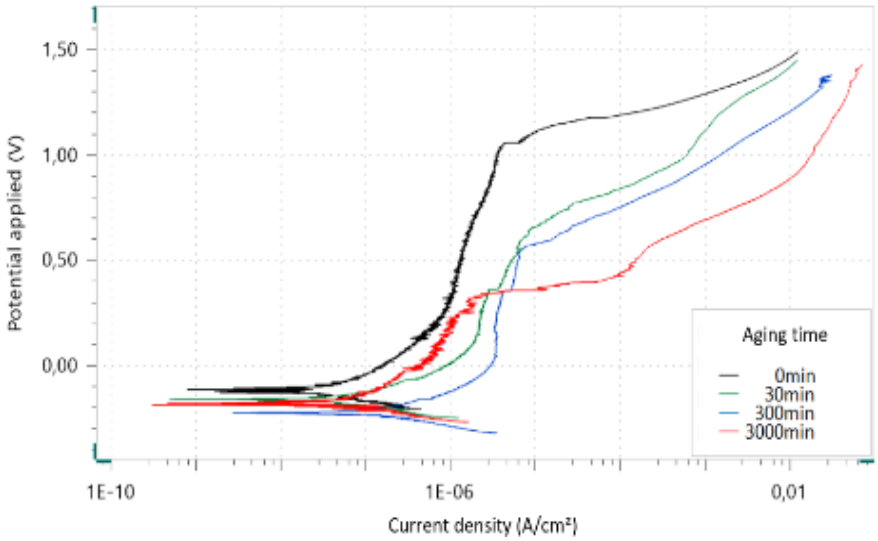

Figure 5: Potentiodynamic polarization curves of UNS S82441 LDSS, in 3.0% NaCl solution (room temperature).

Tested UNS S82441 LDSS showed a typical anodic polarization behavior of a stainless steel in a NaCl solution consisting of active dissolution, passivity, and increase in the current density due to pitting. This rapid increase in the current density indicates the occurrence of the stable pitting in which the potential corresponding to this current transient is known as a critical pitting potential, E_{pit} [13-15]. In Figure 5 some current density spikes are observed at potentials below E_{pit} for the sample aged 3000 minutes. These spikes are due to the occurrence of metastable pits and are explained by the consecutive formation and repassivation of micro size pits [13-15].

Table 5 summarizes the current densities and the potentials determined from the polarization curves in Figure 5, for comparison. All of the polarization curves were evaluated by Tafel extrapolation of Tafel regions to obtain I_{corr}.

Table 5: Potentials and current densities obtained for the aged UNS S82441 LDSS.

SAMPLE	ECOR (MV)	ICOR (A/CM²) 10-8	EPIT (MV)	IPIT (A/CM²) 10-6	PASSIVATION RANGE (MV)
0	-171 ± 82	-4,26 ± 5,32	1081 ± 129	7,46 ± 1,252	1252 ± 121
30	-192 ± 39	-2,99 ± 0,62	583 ± 112	18,50 ± 0,774	774 ± 103
300	-230 ± 13	-3,54 ± 2,43	397 ± 222	5,43 ± 2,130	627 ± 219
3000	-189 ± 23	-2,89 ± 2,35	390 ± 109	5,78 ± 5,301	579 ± 108

The polarization curves, for all the study conditions of the material, present peaks of minimum current density around 10^{-7} A/cm². In the region that the passivation process starts, all the samples evaluated have very similar passivation initiation potential (E_{cor}), about -200mV, and as the passivation process continues, the thermally treated samples present higher current density levels. The as-received material presents a passivation breaking potential (E_{pit}) about 1000 mV, while the aged samples present lower values for the longer times of isothermal aging, reducing the (E_{pit}) values to about 400 mV for samples aged for 300 and 3000 minutes. The same behavior is observed for the passivation range. Increasing the aging time reduces the passivation range from 1200mV (material as received) to about 600mV (material aged for 300 and 3000 minutes), probably due to chromium impoverishment in ferrite grains and grain boundaries, due to the precipitation of sigma phase, deteriorating the corrosion resistance of UNS S82441 LDSS. Therefore, for the test conditions analyzed above, the sample aged for 3000 minutes showed to be less resistant to the corrosive processes, presenting higher current density in relation to the others, in the measurements averages.

The micrographs were obtained after the polarization test with interruption of the test when reaching the potential of E_{pit} to verify the regions where the passivation was initially broken. Figure 6 is a laser confocal microscope image of a test samples showing stable pits and intergranular corrosion grown during the potentiodynamic polarization. Figure 6a show that the passivation breaking process occurs initially in the grain boundaries.

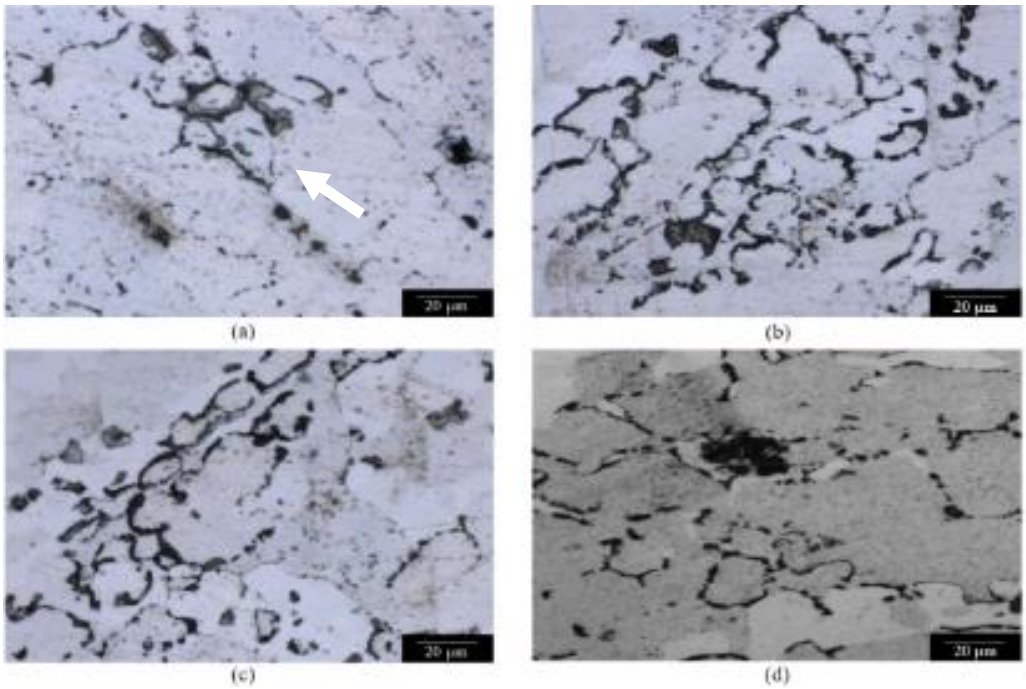

Figure 6: Pits and intergranular corrosion formed on UNS S82441 during the potentiodynamic polarization (1000X): (a) as-received; aged at 850°C for: (b) 30 minutes; (c) 300 minutes; (d) 3000 minutes.

3.3 Stress Corrosion Cracking Tests

Stress corrosion cracking tests (SCC) on specimens, U-Bend type, immersed in 43% $MgCl_2$ solution at 155°C, for 24 hours, were done following the methodology indicated in the standard ASTM G36. This is an accelerated test method for ranking the relative degree of stress corrosion cracking susceptibility for stainless steel. The materials were tested in the as-received and aged conditions. All specimens were stressed parallel to the rolling direction. The stressed parts of U-bend specimens were exposed to the boiling solution for 24 hours and the temperature was maintained at 155°C (adding small amounts of distilled water). The specimens were evaluated by visual inspection, and inspected using dye penetrant examination (at intervals of 8 hours) for the presence of cracks due to SCC. Table 6 summarizes the experimental parameters for the stress corrosion cracking tests.

Table 6: Results for the SCC tests.

SAMPLE TIME AGED (MIN)	CRACKED SPECIMENS				NO CRACKED
	0h	8h	16h	24h	
0	0	0	0	50%	50%
30	0	0	0	100%	0
300	0	0	50%	50%	0
3000	100%	-	-	-	0

The test specimens aged for 3000 min cracked during bending, indicating high embrittlement due to the increase in the level of sigma precipitate. In general, lower resistance to stress corrosion is observed for higher levels of precipitation.

3.4 Mass Loss Tests

Table 7 presents the mass loss values by immersion in iron chloride solution ($FeCl_2$) in a water bath at 50°C for 24 hours. The increase of the corrosion rate occurs due to the increase of the volumetric fraction of the sigma phase.

Table 7: Results for the mass loss test in UNS S82441 LDSS.

AGED TIME (MIN)	ΔMASS (G)	AREA (CM²)	CORROSION RATE (G/CM²)	SIGMA (%)
0	0,2682	23,92	112,12	0
30	0,3022	23,92	126,33	1,89% ± 0,81
300	0,4080	23,92	170,59	4,51% ± 1,41
3000	1,6050	23,92	671,06	20,14% ± 2,52

From the analysis of the graph of Figure 7, the increase of the corrosion rate is verified as a function of the increase of the volumetric fraction of sigma phase in the microstructure of the studied material.

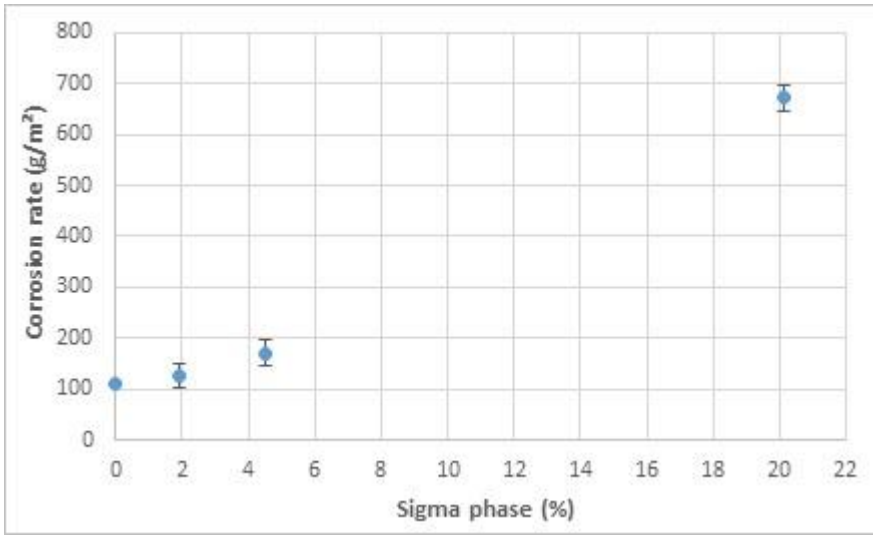

Figure 7: Corrosion rate variation (g/m²) as a function of sigma phase fraction (%).

Figure 8 shows the presence of pits in test specimens tested under all conditions. The amount of pitting and depth of pitting increases with increasing aging time.

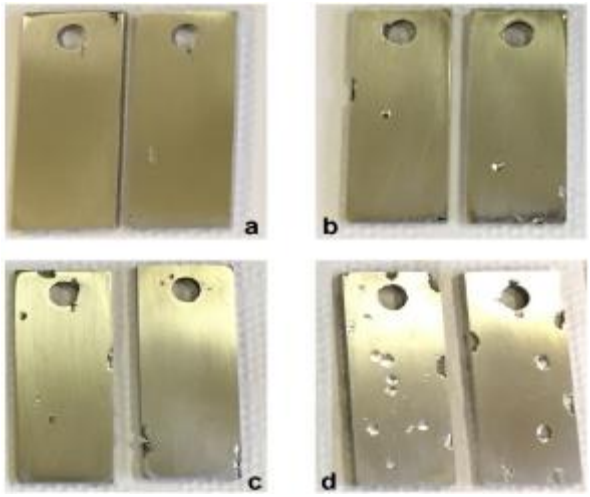

Figure 8: Test specimens after mass loss test. (a) as-received; aged at 850°C (b) 30 min; (c) 300 min; (d) 3000 min

4. CONCLUSIONS

The as-received material contains two phases in approximately equal volume fractions: ferrite (δ) and austenite (γ) and did not present precipitates in its microstructure. This indicates that the material was supplied in

the solution annealed condition.

At the temperature of 850°C, for all aging times, a change in the microstructure of the material is observed, with an increasing in sigma phase content for longer times of aging. According to a previously expected result (since σ = 1.89% aging for 30 minutes, to σ = 20.14% aging for 3000 minutes). The sigma intermetallic phase initially appeared at the ferrite/austenite boundaries and grew inside the ferrite, reducing the fraction of ferrite since δ = 51.91% (as-received) to 23.36% (aged for 3000min).

In the potentiodynamic polarization tests, the exposure of the material to a temperature of 850°C affected the passivation of the material compared to as-received material. The condition aged at 850°C for 3000 minutes reduced the passivation range to 50%. Thus, confirming that the exposure time of this steel at high temperatures decrease its corrosion resistance due to the higher level of sigma precipitation observed.

It has also been proven that intergranular corrosion occurs due to the formation of phase deleterious (sigma), through exposure of the steel to specific temperatures and times, causing embrittlement of the material and greater susceptibility to stress cracking corrosion.

The higher sigma phase content decreased the resistance to pitting and increased the corrosion rate of the material, as verified in the mass loss test.

5. BIBLIOGRAPHY

[1] GUNN, R.N., *Duplex Stainless Steels Microstructure, Properties and Applications*, Cambridge, UK, Abington Publishing 1997.

[2] CHARLES, J., "*Why and Where Duplex Stainless Steels*," Duplex Steels'97, Maastrisht-The Netherlands, 1997.

[3] LO, K. H., SHEK, C. H., LAI, J. K. L., "Recent Developments in Stainless Steels", *Materials Science and Engineering R*, v. 65, pp. 39–104, 2009.

[4] PADILHA, A. F., AGUIAR, D. J. M., PLAUT, R. L., "Duplex Stainless Steels: a Dozen of Significant Phase Transformations", *Defect and Diffusion Forum* v. 322, pp. 163-174, 2012.

[5] IMOA, "Pratical Guidelines for the Fabrication of Duplex Stainless Steels," International Molybdenum Association, 3rd ed., 68p, 2014.

[6] BREDA, M., PELLIZARI, M., FRIGO, M., "σ-Phase in Lean Duplex Stainless Steels Sheets", *Acta Metallurgica Sinica (English Letters)*, pp. 331-337, 2015.

[7] HSIEH, CC, WU, W., "International Scholarly Research Network Metallurgy", 2012:732471, 2012.

[8] MAGNABOSCO, R., "Kinetics of Sigma Phase Formation in a Duplex Stainless Steel", *Materials Research*, v. 12 , n.3, pp. 321-327, 3009.

[9] STRADOMSKI, Z., DYJA, D., "Sigma Phase Precipitation in Duplex Phase Stainless Steel", *Scientific Research*, v. 3, pp. 17-18, 2009.

[10] ROCHA, A.C., SANTOS, A.P.R.S., PEREIRA, G.R., "High Temperature In-Situ X-Ray Analysis of a Lean Duplex Stainless Steel", In: *Proceedings of the 3rd Pan American Materials Congress*, pp. 289-295, 2017.

[11] OUTOKUMPU STAINLESS AB, "*Duplex stainless steel LDX 2404™*", Outokumpu Stainless AB, Avesta Research Centre, 1447EN-GB:2 Centrumtryck AB, September, 2010.

[12] ARQUES, I.J., VICENTE, A.A., TENORIO, J.A.S., *et al*., "Double Kinetics of Intermetallic Phase Precipitation in UNS S32205 Duplex Stainless Steels Submitted to Isothermal Heat Treatment", *Mat. Res.*, pp. 1516-1439, 2016.

[13] YI, Y., CHO, P., AL ZAABI, A., *et al*., "Potentiodynamic Polarization Behaviour of AISI type 316 Stainless Steel in NaCl Solution", *Corrosion Science* vol. 74, pp. 92-97, 2013.

[14] SZKLARSKA-SMIALOWSKA, Z., "Pitting Corrosion of Aluminum", *Corrosion Science* vol. 41, pp. 1743–1767, 1999.

[15] PESSALL, N., LIU., C., "Determination of Critical Pitting Potentials of Stainless Steels in Aqueous Chloride Environments", *Electrochimica Acta* , v. 16, pp. 1987–2003, 1971.

[16] ALVAREZ-ARMAS, I., DEGALLAIX-MOREUIL, S., *Duplex Stainless Steels*, Hoboken, USA, Wiley-Interscience, 2009.

ORCID

Daniel Amâncio Cavalcanti http://orcid.org/0000-0002-2736-5312
Palloma Vieira Muterlle http://orcid.org/0000-0002-7890-4523
Gustavo Reinke http://orcid.org/0000-0001-7457-0864